Amorphous exchange-spring magnets with crossed perpendicular and in-plane anisotropies

K. A. Thórarinsdóttir,[1] T. Hase,[2] B. Hjörvarsson,[3] and F. Magnus[1,*]
[1]*Science Institute, University of Iceland, Dunhaga 3, IS-107 Reykjavik, Iceland*
[2]*Department of Physics, University of Warwick, Coventry CV4 7AL, United Kingdom*
[3]*Department of Physics and Astronomy, Uppsala University, Box 530, SE-75121 Uppsala, Sweden*

(Received 8 September 2020; accepted 13 January 2021; published 25 January 2021)

We study the magnetic coupling in a thin film bilayer exchange-spring magnet composed of an amorphous $Tb_{10}Co_{90}$ layer with a large perpendicular anisotropy and an amorphous $Co_{85}(Al_{70}Zr_{30})_{15}$ layer with uniaxial in-plane anisotropy. The CoAlZr is directly exchange coupled to the TbCo with an interface region of at least 7.5 nm within which the CoAlZr magnetization is perpendicular to the plane and switches with the underlying TbCo. The influence of the coupling extends up to 30 nm into the CoAlZr resulting in an effective tilted anisotropy. The coercivity of the CoAlZr is greatly enhanced due to the coupling and is tuneable over a large range by varying its thickness.

DOI: 10.1103/PhysRevB.103.014440

I. INTRODUCTION

Exchange-spring magnets are composite systems where a hard magnetic layer is coupled through interfacial exchange coupling to a magnetically softer layer. The resulting composite can have the high remanent magnetization of the soft layer as well as the high coercive field of the hard layer. The high energy product is beneficial both for permanent magnets and magnetic storage media. Exchange-spring magnets, where both layers have in-plane magnetic anisotropy (IMA), have been studied extensively [1–3], and it has been shown that the switching properties can be tuned by varying the anisotropy and thickness of the two layers [4,5] as well as the interface structure [6,7]. Spring magnets with perpendicular magnetic anisotropy (PMA) have also been studied and are used in perpendicular magnetic recording [8,9].

In any recording media there is a tradeoff between achieving thermal stability and low switching fields (write fields) when increasing areal density. As the size of the magnetic grains is reduced beyond a certain limit they become thermally unstable and this is referred to as the superparamagnetic limit [10]. Perpendicular recording has allowed materials with higher anisotropy to be used, thus increasing stability compared to longitudinal media [9]. However, a drawback to using a fully PMA layer in magnetic recording media is the high switching field needed to reverse the magnetization. A potential solution to this limitation is to use heat-assisted switching, where the material is temporarily heated to its ordering temperature to reduce its coercive field [11]. Another suggestion to increase areal density and lower the switching field is to use thin films with tilted magnetization [12]. Thin films where the magnetic moment is tilted from the film plane have been achieved by growing magnetic layers on curved nanoislands [13,14] by growing the film such that the film grains are at an angle from the substrate [15] or by making composite systems with mixed magnetic anisotropies [16,17].

In the present study, we examine the magnetic properties of amorphous heterostructures composed of two exchange coupled layers with IMA and PMA. Amorphous materials are highly uniform and free of point defects and step edges, which makes them ideally suited to magnetic heterostructures [18]. The magnetic anisotropy of amorphous thin films can be tuned both by growing the samples in a constant magnetic field or tailoring their composition [19]. Furthermore, strong interfacial exchange coupling has been demonstrated in amorphous heterostructures resulting, for example, in large magnetic proximity effects [3] and magnetic leverage effects [20]. Therefore, there is great potential for engineering amorphous heterostructures so that they display a specific complex magnetic response [3]. Here, we examine how the PMA of a TbCo layer results in a tilted magnetization of a coupled soft CoAlZr layer with imprinted uniaxial IMA. TbCo is known to have a strong growth induced PMA and exhibit all-optical magnetic switching [21]. We determine the range of the direct exchange coupling between the two layers and its effect on the overall magnetic response of the composite system. We find that the extension of the coupled region is large which can be used to control the effective anisotropy of the bilayer.

II. EXPERIMENTAL METHODS AND DESIGN

The samples were grown using dc magnetron sputtering in a sputtering chamber with a base pressure below 5×10^{-9} mbar. The sputtering gas was Ar of 99.9999% purity and growth pressure 2.00×10^{-3} mbar. The Si(001) substrates (with the native oxide layer intact) were annealed in vacuum at 200 °C for 30 min prior to growth. First, a 2-nm-thick buffer layer of $Al_{70}Zr_{30}$ was deposited from an $Al_{70}Zr_{30}$ alloy target. Next, a bilayer of $Tb_{10}Co_{90}$ and $Co_{85}(Al_{70}Zr_{30})_{15}$ was grown by co-sputtering from Co (purity 99.9%), Tb (purity 99.9%),

*fridrikm@hi.is

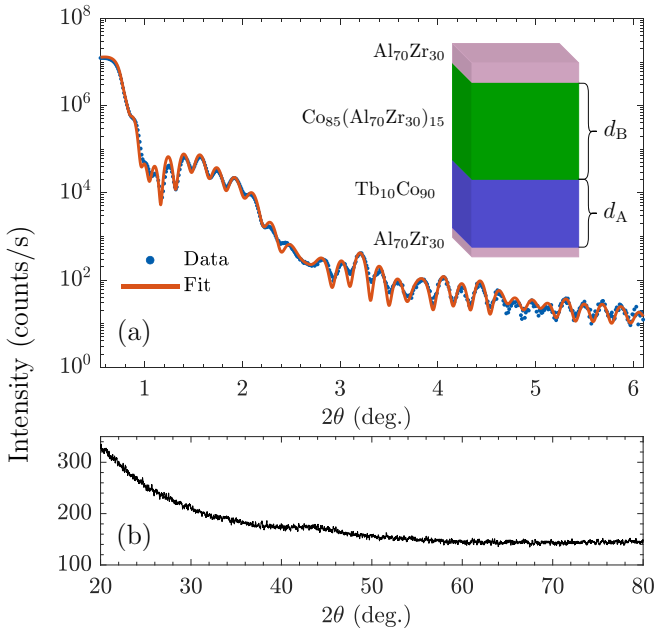

FIG. 1. (a) A representative XRR measurement including a fit, showing the low interface roughness of the bilayers. The inset shows a schematic of the sample structure corresponding to the measurement, where $d_A = 30$ nm and $d_B = 15$ nm. (b) A GIXRD measurement of the same sample, showing a single broad peak at approximately $2\theta = 45°$. The measurement is representative of the entire sample series.

and $Al_{70}Zr_{30}$ alloy targets. Finally, all samples were capped with 4-nm $Al_{70}Zr_{30}$. The sample structure is shown in the inset of Fig. 1(a).

The amorphous atomic structure of the samples was confirmed using grazing incidence x-ray diffraction (GIXRD) and the layer thicknesses and interface roughnesses determined by x-ray reflectivity (XRR). Characteristic XRR, including a fit, and GIXRD are shown in Figs. 1(a) and 1(b), respectively. The XRR shows Kiessing fringes up to at least $2\theta = 6°$, confirming low interface roughness. Fitting the data confirms that the actual thicknesses agree with the nominal ones. A typical root-mean-square interface roughness is 0.6 nm between the TbCo and CoAlZr layers, allowing us to rule out intermixing effects. The GIXRD shows a single broad peak at approximately $2\theta = 45°$ which is characteristic of amorphous structures [19]. More information on the structural characterization methods can be found in Ref. [22].

Vibrating sample magnetometry (VSM) in a longitudinal geometry was used for magnetic characterization. All measurements were carried out at 20 K with applied fields up to 5 T. VSM measures the projection of the total magnetic moment along the measurement axis. In multicomponent magnetic samples the hysteresis loops obtained in this way can be composed of two or more different magnetic responses superimposed.

The samples were grown in a constant in-plane magnetic field of approximately 130 mT which induces a uniaxial in-plane magnetic anisotropy (IMA) in the CoAlZr layer. To study how the strong PMA from the TbCo affects the soft IMA CoAlZr, a series of samples were grown with the TbCo thickness fixed at 30 nm and the CoAlZr thickness ranging between 5 and 80 nm. For a few thicknesses, additional samples were made with a 2.5-nm-thick AlZr spacer layer inserted between the TbCo and CoAlZr layers. This allows us to separate the effects of direct exchange coupling and stray field coupling on the magnetic response [17]. It has been demonstrated previously that there is no interlayer exchange coupling through amorphous $Al_{70}Zr_{30}$ layers of this thickness through either RKKY coupling or proximity induced magnetism [23].

III. RESULTS AND DISCUSSION

Out-of-plane and in-plane hysteresis loops of single CoAlZr and TbCo layers are shown in Figs. 2(a) and 2(b), respectively. The CoAlZr has a square hysteresis loop along its in-plane easy axis, defined by the applied growth field, with a low coercive field (<10 mT) while in the perpendicular in-plane direction the remanence is zero (not shown). In the out-of-plane direction it has a high saturation field of 1.1 T and zero remanence. This shows that it has a small but well-defined uniaxial IMA.

The TbCo has a square hysteresis loop in the out-of-plane direction with $H_c = 190$ mT. In the in-plane direction the saturation field is above the highest available field of 5 T. Therefore it has a large PMA, although the small nonzero remanence in the in-plane direction suggests that there is a small component of the film with less well defined anisotropy, which increases when growing the samples in a constant in-plane magnetic field [24]. TbCo and TbFe are ferrimagnets which are known to have a strong PMA. It has been suggested that the origin of the PMA in amorphous TbFe thin films is short-range structural ordering, similar to texturing in polycrystalline films, which is a result of minimization of the surface energy during deposition [25]. The structural and magnetic anisotropy is strongly correlated, where the Tb-Fe pair correlations are found to be larger out-of-plane, while Fe-Fe and Tb-Tb correlations are greater in-plane [26]. A similar effect can be expected in TbCo. The antiparallel alignment of the Tb and Co magnetic moments results in a compensation temperature (where the magnetization is zero and the coercivity diverges) when the magnetic moments cancel. This compensation temperature varies with composition [24].

Putting the TbCo and CoAlZr layers together with a nonmagnetic AlZr spacer layer we obtain the magnetic response shown in Fig. 2(c). The hysteresis loop measured out of plane is a sum of the square easy-axis loop corresponding to the TbCo and the hard-axis loop of the CoAlZr. This is clear from the fact that the coercivity matches that of the TbCo and the saturation field matches that of the CoAlZr. Additionally, there is a small step at roughly 10 mT, corresponding to approximately 2% of the total CoAlZr moment. Since there is no direct exchange coupling, the step has to originate from magnetic anisotropy. During growth we apply a magnetic field of 130 mT parallel to the film plane, but in addition the CoAlZr layer experiences a large stray field from the TbCo. On this length scale, the stray field is uniform, so the total field is approximately uniform and tilted at an unknown angle with respect to the plane. CoAlZr is susceptible to field imprinting of anisotropy during growth [3], and therefore a small tilting

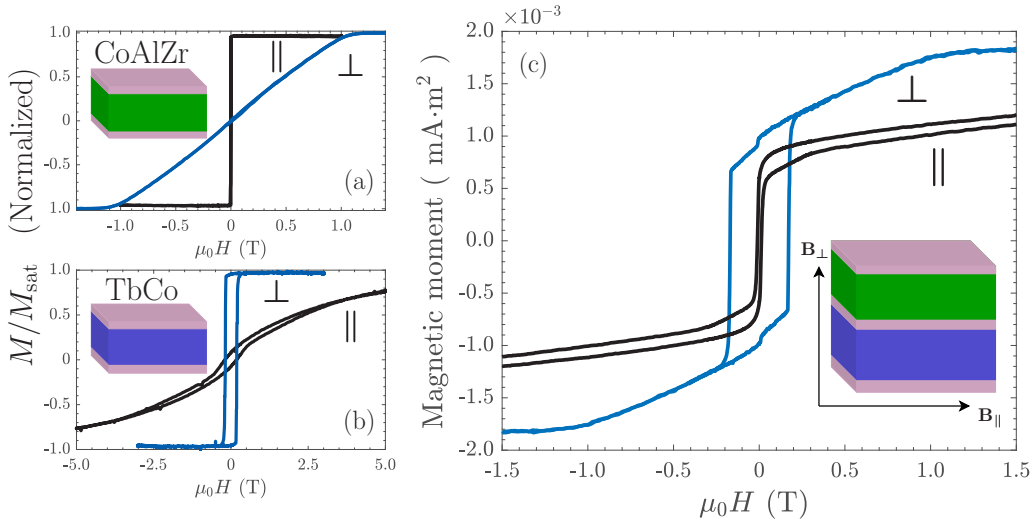

FIG. 2. Magnetic hysteresis loops measured by VSM in the out-of-plane and in-plane directions on (a) a single layer of CoAlZr and (b) a single layer of TbCo. The TbCo has a well-defined PMA whereas the CoAlZr has a clear uniaxial IMA. (c) The magnetic response of a TbCo(30 nm)/AlZr(2.5 nm)/CoAlZr(15 nm) sample, measured both in-plane and out-of-plane by VSM. The AlZr spacer layer decouples the two magnetic layers such that they switch independently. Data are shown between −1.5 T to 1.5 T for clarity, with the measurement extending to ±5 T.

of the anisotropy out of the plane can result. From the size of the magnetization step we estimate that the in-plane easy axis is tilted out of the plane by approximately 1°. The in-plane measurement is a sum of a square loop with a low coercive field and a hard-axis loop with a slight opening and saturation field above 5 T. At zero field, the remanence measured in-plane and out-of-plane corresponds to the magnetic moment of the CoAlZr and TbCo layers, respectively. This shows that the two layers switch independently when there is no direct exchange coupling and the effect of the stray field from the TbCo on the CoAlZr is minimal.

Samples without an AlZr spacer layer have direct coupling between the two magnetic layers. A schematic of this sample structure is shown in the inset of Fig. 1(a). The TbCo thickness d_A is fixed at 30 nm for all samples and the CoAlZr thickness d_B ranges from 5 nm to 80 nm. Figures 3(a) and 3(b) show hysteresis loops out-of-plane and in-plane, respectively, for various d_B, including the single TbCo layer for reference ($d_B = 0$). With increasing thickness of the CoAlZr the out-of-plane response gradually evolves from the square response characteristic of a PMA material to a mixed easy and hard axis response. Similarly, the in-plane hysteresis loops acquire an increasingly large component which switches abruptly at low field with an associated increase in the remanent magnetization.

The hysteresis loops in Fig. 3 are the response of a multicomponent system with different anisotropies and magnetic moments. In order to separate these different responses we fit the hysteresis loops with a sum of modified Langevin functions of the form

$$M = A\left(\frac{1}{\tanh\frac{H\pm H_C}{S}} - \frac{1}{\frac{H\pm H_C}{S}}\right), \quad (1)$$

where A is the saturation moment, H_C is the coercive field, S determines the shape of the loop, and H is the applied field. The equation has no theoretical basis but can capture the key parameters defining complex magnetic hysteresis loops. The fit is unique in cases where one or more square loops and an S-shaped (hard axis) loop is combined but can yield nonunique solutions when separating hysteresis loops that are a mixture of many hard responses saturating at different fields. By fitting the measured data with Eq. (1), we are able to separate the contribution from the two layers and extract robust values for the saturation moment and coercivity. In the out-of-plane direction, we find that for the smallest d_B only one hyperbolic function is required to fit the magnetic response, but for larger d_B a sum of two hyperbolic functions is needed to obtain a satisfactory fit. An example of this case is shown in Figs. 4(a) and 4(b). The total response is composed of a square loop with a large remanence and coercivity and a smooth S-shaped loop with zero remanence and a high saturation field. The low field step seen in Fig. 2(c) does not appear in the coupled system due to the strong direct exchange coupling between the TbCo and CoAlZr which dominates over the effect of the stray field.

Figure 4(c) shows the saturation moment of the two components forming the out-of-plane response plotted as a function of d_B. For the smallest CoAlZr thicknesses, there is only a square component and its saturation moment increases with increasing d_B. Above a certain threshold, the S-shape component appears and its saturation moment increases linearly with increasing d_B and the square component remains constant. This shows that part of the CoAlZr layer, below a threshold thickness, is strongly coupled to the TbCo layer and acts as an extension to the PMA layer. This is further borne out by the fact that the remanence of the square component equals its saturation moment, showing that this CoAlZr interface layer remains out-of-plane in the absence of an applied field. As the thickness of the CoAlZr exceeds the threshold, the magnetic moment within the CoAlZr layer beyond this threshold falls back into the film plane. By extrapolating the linear dependence of the saturation moment of the

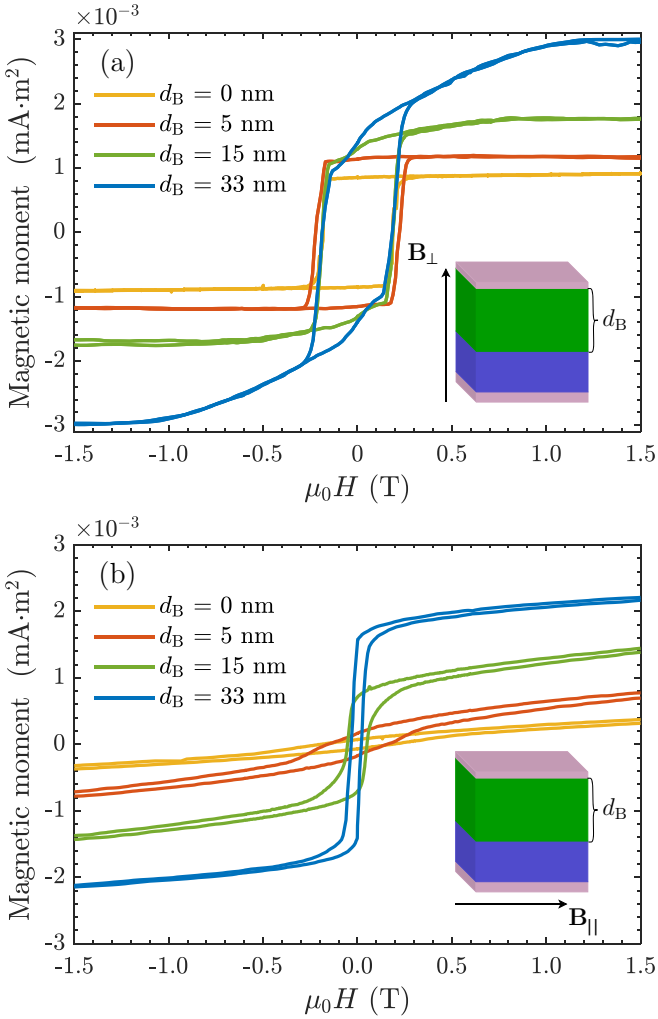

FIG. 3. The magnetic response of TbCo/CoAlZr bilayers with crossed anisotropies measured by VSM. (a) Out-of-plane hysteresis loops. (c) In-plane hysteresis loops, parallel to the growth field direction (in-plane easy axis). The data shown are between ±1.5 T for clarity, with the measurements extending to ±5 T.

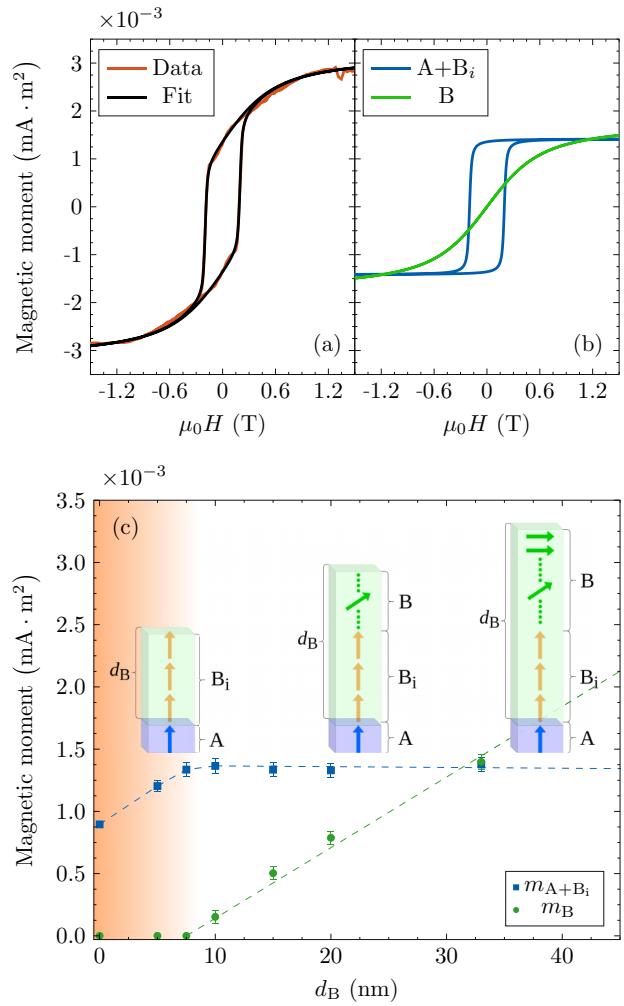

FIG. 4. (a) The hysteresis loop of a bilayer with $d_B = 33$ nm (red) perpendicular to the plane. The data is fitted using Eq. 1 resulting in the solid black line. The fit is composed of two loops, shown in (b), a square loop and an S-shaped loop, corresponding to different components of the bilayer. (c) The saturation moment of the different components extracted from fitting the VSM data, as depicted in (a) and (b). The (blue) squares and (green) circles correspond to the square and S-loop, respectively. Up until $d_B = 7.5$ nm there is no contribution from the hard axis loop, indicating that at least 7.5 nm of the soft CoAlZr switches with the TbCo. The dashed lines are a guide to the eye and extend to $d_B = 80$ nm (not shown). The insets show the different magnetic components schematically.

CoAlZr we can determine the thickness of the interface layer, which is strongly coupled to the TbCo to be (7.5 ± 0.2) nm. The excess out-of-plane saturation moment can similarly be determined to be $(4.4 \pm 0.4) \times 10^{-4}$ mA m^2 which corresponds to a CoAlZr layer of thickness 8.4 ± 0.7 nm.

Although the CoAlZr interface layer switches in unison with the TbCo layer when the field is applied perpendicular to the plane, it clearly has a magnetic response which is distinct from the TbCo. This becomes clear by studying the in-plane hysteresis loops in Fig. 3(b). These loops are composed of at least two "hard" loops, and an increasingly large "soft" loop emerges beyond $d_B = 7.5$ nm. Due to nonuniqueness of the fit we cannot with certainty ascribe a magnetic moment separately to the two "hard" responses. However, the fitting allows us to identify three different regions of the sample. The first [labelled 'A' in the insets of Fig. 4(c)] is the PMA TbCo layer with a large in-plane saturation field (≈ 4.5 T) and a small in-plane remanence. The second (labelled 'B$_i$') corresponds to the CoAlZr interface region up to $d_B = 7.5$ nm, with a weaker effective PMA characterized by an intermediate in-plane saturation field. The third (labelled 'B') is the CoAlZr beyond $d_B = 7.5$ nm, where a crossover from PMA to IMA occurs. These different magnetic regions are depicted in a simple schematic in the insets of Fig. 4(c). We stress that the schematic is not a definitive representation of the remanent spin state of the bilayers and does not depict domain structure. In fact, the remanent state is metastable and depends on the field history of the sample.

Although the interface region B$_i$ has a thickness of approximately 7.5 nm the influence of the exchange coupling

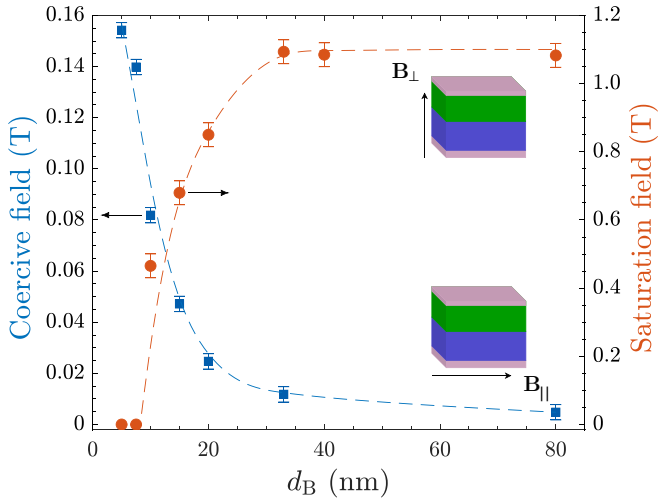

FIG. 5. (Left) Coercive field of hysteresis loops measured in-plane [Fig. 3(c)] as a function of thickness. For thin d_B the coercivity is enhanced by two orders of magnitude compared to bulk CoAlZr. (Right) The saturation field of the S-shape (hard axis) component loop from the out-of-plane measurement [Fig. 3(b)] plotted as a function of d_B. The field required to saturate the CoAlZr out-of-plane is significantly reduced for thicknesses below $d_B = 33$ nm. Dashed lines are a guide to the eye.

between the TbCo and CoAlZr layers extends far beyond this thickness. Figure 5 shows the saturation field of the S-shape (hard axis) component of the *out-of-plane* hysteresis loops [Fig. 3(a)] and the coercive field when measuring *in-plane* [Fig. 3(b)], for different CoAlZr thicknesses d_B. These parameters reflect the influence that the coupling to the TbCo has on the properties of the CoAlZr. The influence of the coupling will decay with distance from the interface and the field required to rotate the CoAlZr moments out of the plane will vary continuously from the interface to the surface. The out-of-plane saturation field is therefore a measure of the strength of the coupling between the TbCo and the surface of the CoAlZr. For small d_B they are strongly coupled and the saturation field is strongly reduced, allowing the moments of the CoAlZr to be rotated perpendicular to the plane in relatively small fields. This influence decreases with increasing d_B but only reaches the "bulk" value for CoAlZr (determined by shape anisotropy) for $d_B > 33$ nm. This long-range influence is a result of the direct exchange coupling and not stray field coupling as demonstrated in the samples with a nonmagnetic spacer. This is further supported by the coercive field of the in-plane hysteresis loops. For small d_B the in-plane coercive field of the CoAlZr is enhanced by two orders of magnitude compared to its "bulk" value. For increasing d_B the coercive field decreases sharply but does not approach the bulk value until $d_B > 33$ nm. This demonstrates the strong coupling in a bilayer system with crossed anisotropies and how it can be used to tune the switching properties and effective anisotropy both in-plane and perpendicular to the plane.

IV. CONCLUSIONS

A series of amorphous samples with crossed magnetic anisotropies was investigated in bilayered systems of TbCo (30 nm)/CoAlZr (5–80 nm). Due to the strong direct exchange coupling between the layers, a 7.5 nm thick region of the CoAlZr layer is pinned perpendicular to the plane and acts as an extension of the TbCo. The coercive field of the normally soft CoAlZr layer is strongly enhanced throughout a distance of at least 30 nm from the TbCo/CoAlZr interface, and in this region it acquires an effective tilted anisotropy. These results demonstrate the power of combining amorphous magnetic layers with widely different magnetic properties. The combination of seamless interfaces and susceptibility to field imprinting of anisotropy results in an unusually long-range coupling between the layers. This could be used for engineering high density magnetic recording media with tilted anisotropy as well as in spintronic devices using all-optical or spin-orbit torque-induced magnetic switching.

ACKNOWLEDGMENT

This work was supported by the Icelandic Centre for Research, Grant No. 174271-051, and the University of Iceland Research Fund.

[1] E. E. Fullerton, J. S. Jiang, C. Rehm, C. H. Sowers, S. D. Bader, J. B. Patel, and X. Z. Wu, High coercivity, epitaxial Sm-Co films with uniaxial in-plane anisotropy, Appl. Phys. Lett. **71**, 1579 (1997).

[2] E. E. Fullerton, J. S. Jiang, M. Grimsditch, C. H. Sowers, and S. D. Bader, Exchange-spring behavior in epitaxial hard/soft magnetic bilayers, Phys. Rev. B **58**, 12193 (1998).

[3] F. Magnus, M. E. Brooks-Bartlett, R. Moubah, R. A. Procter, G. Andersson, T. P. A. Hase, S. T. Banks, and B. Hjörvarsson, Long-range magnetic interactions and proximity effects in an amorphous exchange-spring magnet, Nat. Commun. **7**, 11931 (2016).

[4] S.-S. Yan, J. A. Barnard, F.-T. Xu, J. L. Weston, and G. Zangari, Critical dimension of the transition from single switching to an exchange spring process in hard/soft exchange-coupled bilayers, Phys. Rev. B **64**, 184403 (2001).

[5] Z. J. Guo, J. S. Jiang, J. E. Pearson, S. D. Bader, and J. P. Liu, Exchange-coupled Sm-Co/Nd-Co nanomagnets: correlation between soft phase anisotropy and exchange field, Appl. Phys. Lett. **81**, 2029 (2002).

[6] Y. Liu, S. G. E. te Velthuis, J. S. Jiang, Y. Choi, S. D. Bader, A. A. Parizzi, H. Ambaye, and V. Lauter, Magnetic structure in Fe/Sm-Co exchange spring bilayers with intermixed interfaces, Phys. Rev. B **83**, 174418 (2011).

[7] Y. Choi, J. S. Jiang, J. E. Pearson, S. D. Bader, J. J. Kavich, J. W. Freeland, and J. P. Liu, Controlled interface profile in Sm-Co-Fe exchange-spring magnets, Appl. Phys. Lett. **91**, 072509 (2007).

[8] S. M. Watson, T. Hauet, J. A. Borchers, S. Mangin, and E. E. Fullerton, Interfacial magnetic domain wall formation in perpendicular-anisotropy, exchange-spring films, Appl. Phys. Lett. **92**, 202507 (2008).

[9] A. Berger, N. Supper, Y. Ikeda, B. Lengsfield, A. Moser, and E. E. Fullerton, Improved media performance in optimally coupled exchange spring layer media, Appl. Phys. Lett. **93**, 122502 (2008).

[10] R. Wood, The feasibility of magnetic recording at 1 terabit per square inch, IEEE Trans. Magn. **36**, 36 (2000).

[11] R. E. Rottmayer, S. Batra, D. Buechel, W. A. Challener, J. Hohlfeld, Y. Kubota, L. Li, B. Lu, C. Mihalcea, K. Mountfield *et al.*, Heat-assisted magnetic recording, IEEE Trans. Magn. **42**, 2417 (2006).

[12] J. P. Wang, Y. Y. Zou, C. H. Hee, T. C. Chong, and Y. F. Zheng, Approaches to tilted magnetic recording for extremely high areal density, IEEE Trans. Magn. **39**, 1930 (2003).

[13] M. Albrecht, G. Hu, I. L. Guhr, T. C. Ulbrich, J. Boneberg, P. Leiderer, and G. Schatz, Magnetic multilayers on nanospheres, Nat. Mater. **4**, 203 (2005).

[14] M. Albrecht, Magnetic films on nanoparticle arrays, The Open Surface Science Journal **4**, 42 (2012).

[15] B. Ma, H. Wang, H. Zhao, C. Sun, R. Acharya, and Jian-ping Wang, Structural and magnetic properties of a core-shell type L10 FePt/Fe exchange coupled nanocomposite with tilted easy axis, J. Appl. Phys. **109**, 083907 (2011).

[16] S. Łazarski, W. Skowroński, J. Kanak, Ł. Karwacki, S. Zietek, K. Grochot, T. Stobiecki, and F. Stobiecki, Field-free spin-orbit-torque switching in Co/Pt/Co multilayer with mixed magnetic anisotropies, Phys. Rev. Applied **12**, 014006 (2019).

[17] D. Markó, F. Valdés-Bango, C. Quirós, A. Hierro-Rodríguez, M. Vélez, J. I. Martín, J. M. Alameda, D. S. Schmool, and L. M. Álvarez Prado, Tunable ferromagnetic resonance in coupled trilayers with crossed in-plane and perpendicular magnetic anisotropies, Appl. Phys. Lett. **115**, 082401 (2019).

[18] P. T. Korelis, A. Liebig, M. Bjorck, B. Hjorvarsson, H. Lidbaum, K. Leifer, and A. R. Wildes, Highly amorphous $Fe_{90}Zr_{10}$ thin films, and the influence of crystallites on the magnetism, Thin Solid Films **519**, 404 (2010).

[19] F. Magnus, R. Moubah, A. H. Roos, A. Kruk, V. Kapaklis, T. Hase, B. Hjorvarsson, and G. Andersson, Tunable giant magnetic anisotropy in amorphous SmCo thin films, Appl. Phys. Lett. **102**, 162402 (2013).

[20] R. A. Procter, F. Magnus, G. Andersson, C. Sánchez-Hanke, B. Hjörvarsson, and T. Hase, Magnetic leverage effects in amorphous smco/coalzr heterostructures, Appl. Phys. Lett. **107**, 062403 (2015).

[21] A. Ciuciulkaite, K. Mishra, M. V. Moro, I.-A. Chioar, R. M. Rowan-Robinson, S. Parchenko, A. Kleibert, B. Lindgren, G. Andersson, C. S. Davies, A. Kimel, M. Berritta, P. M. Oppeneer, A. Kirilyuk, and V. Kapaklis, Magnetic and all-optical switching properties of amorphous Tb_xCo_{100-x} alloys, Phys. Rev. Materials **4**, 104418 (2020).

[22] K. A. Thórarinsdóttir, H. Palonen, G. K. Palsson, B. Hjörvarsson, and F. Magnus, Giant magnetic proximity effect in amorphous layered magnets, Phys. Rev. Materials **3**, 054409 (2019).

[23] Yu Fu, I. Barsukov, H. Raanaei, M. Spasova, J. Lindner, R. Meckenstock, M. Farle, and B. Hjörvarsson, Tailored magnetic anisotropy in an amorphous trilayer, J. Appl. Phys. **109**, 113908 (2011).

[24] A. Frisk, F. Magnus, S. George, U. B. Arnalds, and G. Andersson, Tailoring anisotropy and domain structure in amorphous TbCo thin films through combinatorial methods, J. Phys. D **49**, 035005 (2015).

[25] F. Hellman and E. M. Gyorgy, Growth-Induced Magnetic Anisotropy in Amorphous Tb-Fe, Phys. Rev. Lett. **68**, 1391 (1992).

[26] V. G. Harris, K. D. Aylesworth, B. N. Das, W. T. Elam, and N. C. Koon, Structural Origins of Magnetic Anisotropy in Sputtered Amorphous Tb-Fe Films, Phys. Rev. Lett. **69**, 1939 (1992).